Applied Science and Innovative Research
ISSN 2474-4972 (Print) ISSN 2474-4980 (Online)
Vol. 8, No. 3, 2024
www.scholink.org/ojs/index.php/asir

Original Paper

Research on the Influencing Factors of Pulsed Hydraulic Fracturing Effects in Hot Dry Rock Based on Numerical Simulation

Qinqin Zou[1], Liliang Gong[2] & Ziwang Yu[1*]

[1] College of Construction Engineering, Jilin University, Changchun, 130026, China

[2] Jianghe Anlan Engineering consulting Co., Ltd, Zhengzhou, 450003, China

[*] Corresponding author, Ziwang Yu, College of Construction Engineering, Jilin University, Changchun, 130026, China

E-mail: yuziw@jlu.edu.cn

Received: June 15, 2024 Accepted: July 12, 2024 Online Published: July 17, 2024

doi:10.22158/asir.v8n3p81 URL: http://doi.org/10.22158/asir.v8n3p81

Abstract

Geothermal energy, representing one of the five principal non-carbon-based renewable resources, is crucial in the global energy transition and in mitigating greenhouse gas emissions. Hot Dry Rock (HDR) reservoirs, rich in geothermal resources, predominantly utilize hydraulic fracturing, the most extensively researched and applied technology. However, fracturing these robust HDR formations poses significant challenges compared to traditional hydraulic fracturing in sedimentary rocks in the oil and gas industry. Cyclic pulse fracturing, an innovative mode of fracturing, has received limited academic attention, particularly regarding its permeability enhancement mechanism under varying thermal and pressure conditions, which remains largely unexplored. Building on prior laboratory experiments, this study employs the pore pressure cohesive zone model within ABAQUS software to elucidate the initiation and expansion of hydraulic fractures. Numerical simulations investigated the influence of critical parameters such as pulse pattern, temperature, geostress differential, and confining pressure on fracture propagation. The findings indicate that cyclic pulse hydraulic fracturing can significantly reduce the breakdown pressure in HDR, with reductions up to 37.68% under certain conditions. Notably, at constant amplitude, increased frequency exacerbates damage to hot dry rocks; conversely, at constant frequency, higher amplitudes result in greater damage. Additionally, pulse hydraulic fracturing improves the fracturing process, yielding a more intricate fracture network. In HDR pulse hydraulic fracturing, the temperature disparity between the fracturing fluid and the rock markedly impacts the breakdown pressure. Cold water interacting with a high-temperature geo-thermal reservoir triggers a thermal shock effect, diminishing initiation pressure and expediting fracture

development and expansion. The impact of geostress differential and confining pressure on pulse hydraulic fracturing is complex, influencing not only the breakdown pressure but also the direction and extent of fracture expansion.

Keywords

hydraulic fracturing, hot dry rock, numerical simulation, multistage cyclic pulses

1. Introduction

Geothermal resources encompass geothermal energy, fluids, and their beneficial components found on Earth that can be economically harnessed by humans. These resources are classified into three categories: shallow geothermal resources, hydrothermal resources, and dry-heat rock resources. The latter category comprises high-temperature rock bodies typically exceeding 180 ℃, located at depths of several kilometers, and possessing minimal or no internal subsurface fluids, which are dense and impermeable (Wu et al., 2012; Yang et al., 2023). Geothermal energy is utilized in a variety of applications including power generation, heating and cooling, spa treatments, and industrial processes. As one of the five principal non-carbon-based renewable energy sources, geothermal energy plays a crucial role in facilitating the global energy transition and mitigating greenhouse gas emissions.

Enhanced Geothermal Systems (EGS) are pivotal in developing geothermal resources within dry, hot rock (HDR) formations. The fundamental process involves drilling and fracturing the reservoir to create a sizable and complex fracture network, thereby increasing the permeability of the thermal reservoir formations (Gong et al., 2023). Reservoir modification plays a critical role in various major subterranean energy projects, including EGS, oil shale, and shale gas developments, where hydraulic fracturing emerges as the most extensively researched and applied technology. Unlike traditional oil and gas fields, where sedimentary rocks are subjected to hydraulic fracturing, the technique faces significant challenges when applied to the harder, dry, and hot rock environments typical of HDR.

In exploring hydraulic fracturing methods, Arno Zang introduced the concept of Fatigue Hydraulic Fracturing (FHF) in 2013, proposing various fluid injection schemes, such as cyclic, progressive, and fatigue hydraulic fracturing. This approach, differing from traditional methods with steadily increasing injection pressure, tends to create broader fracture zones, showcasing that varying injection schemes significantly impact hydraulic fracture development (Zang et al., 2013). In 2015, Reza Safari's evaluation of the geomechanical aspects of pulse fracturing through numerical simulations revealed that pulsed loading could lead to a ductile/brittle transition in shale rock's fracture network (Safari et al., 2015). Luke P. Frash furthered this research by hydraulically augmenting granite samples with mechanical impulse hydraulic fracturing (MIHF) as a re-stimulation technique to enhance well injection capacity (Frash et al., 2015). In 2017, Chen et al. employed a three-axis loaded impulse hydraulic fracturing test system to explore the effects of varying pulse frequency and fluid viscosity on coal rock, revealing that pulse hydraulic fracturing promotes mutant crack expansion and reaming effects (Jiang-zhan et al., 2017). Zimmermann et al. conducted tests in the Äspö hard rock laboratory using new cyclic and pulse injection schemes in 2019, followed by an optimization study

(Zimmermann et al., 2018). In 2020, Kang et al. at MIT showed that cyclic fracturing could lower in-situ fracture pressure in sandstone samples (Kang et al., 2020). In 2022, Chang et al. investigated black shale's hydraulic fracturing from the Sichuan Basin's Lower Silurian Longmaxi Formation, employing constant-flow, cyclic, shut-in interval, and low-frequency pulse booster injections. They found cyclic fracturing more likely to induce fatigue damage, creating subcritical microfractures that expand into macrofractures, with cyclic water injection reducing rock fracture pressure by approximately 24%. Although shut-in well intermittent water injection also reduced pressure, it was less effective in enhancing fracture complexity. Pulse fracturing yielded the most intricate fracture patterns among the tested schemes, with rapid pressure changes promoting multiple fractures around the borehole (Chang et al., 2022). Despite these advancements, cyclic pulse fracturing's permeability enhancement mechanisms under various temperatures and pressures remain largely unexplored.

In the current scenario, significant opportunities exist to enhance the permeability optimization of hydraulic fracturing technology for Enhanced Geothermal Systems (EGS) reservoir modification. The hydraulic fracturing process, characterized by varying fluid injection patterns and fluid seepage rates within the rock, generates diverse fracture pressures. By deviating from the conventional constant-flow injection scheme and integrating monitoring arrays within the fracture monitoring site, along with the deployment of efficient pulse and fatigue fracturing techniques, an improved injection strategy can be devised for permeability enhancement. However, these methods are currently in the stages of theoretical exploration and preliminary testing, with engineering construction predominantly reliant on engineers' experience and field feedback, indicating an urgent need for technological advancements. This paper investigates the impact of varying the pulsing pattern, temperature, geostress differences, and confining pressures on the expansion of fractures in dry hot rocks. By comparing fracture pressure, length, and the number of fracture units under diverse conditions, it unveils the pattern of enhanced permeability in dry hot rocks post-hydraulic fracturing. This study offers solutions to complex and practical engineering challenges, facilitating the achievement of optimal fracturing outcomes and guiding engineering practices effectively.

2. Theoretical Background

2.1 Theoretical Foundations

The two-dimensional elastic stresses around a circular cavity within a homogeneous linear elastic solid, as described by Kirsch's well-known solution (1898), can be accurately determined. While the stress state in laboratory triaxial hydraulic fracturing tests inherently involves three dimensions, it can be effectively reduced to a two-dimensional stress state on a planar plate perpendicular to the horizontal drilling axis, as illustrated in Figure 1.

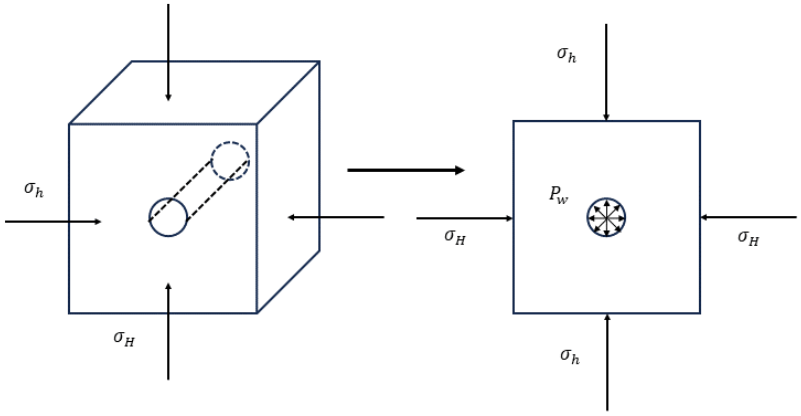

Figure 1. Conversion from 3-D to 2-D

Therefore, we can derive the following equation based on Kirsch's theory:

$$\sigma_r = \frac{(\sigma_H + \sigma_h)(1 - \frac{r_w^2}{r^2})}{2} - \frac{(\sigma_H - \sigma_h)\left(1 - 4\frac{r_w^2}{r^2} + 3\frac{r_w^4}{r^4}\right)\cos 2\theta}{2} + P_w \frac{r_w^2}{r^2} \quad (1)$$

$$\sigma_\theta = \frac{(\sigma_H + \sigma_h)(1 + \frac{r_w^2}{r^2})}{2} - \frac{(\sigma_H - \sigma_h)\left(1 + 3\frac{r_w^4}{r^4}\right)\cos 2\theta}{2} - P_w \frac{r_w^2}{r^2} \quad (2)$$

When the absolute value of σ_θ is greater than the tensile strength T, tensile fracture of the hole wall occurs. Therefore, when $\theta = 0$ or π and $r = r_w$, the breakdown pressure is:

$$P_b = 3\sigma_h - \sigma_H - \sigma_\theta = 3\sigma_h - \sigma_H - T \quad (3)$$

$$\varepsilon_r = \frac{1}{E}(\sigma_r - v\sigma_\theta)$$

$$\varepsilon_\theta = \frac{1}{E}(\sigma_\theta - v\sigma_r) \quad (4)$$

Therefore, we can program MATLAB to calculate the stresses and strains of the single-hole model based on the above equations.

Where σ_r is the radial stress; σ_θ is the tangential stress; ε_r is the radial strain; ε_θ tangential strain; σ_H is the maximum horizontal principal stress; σ_h is the minimum horizontal principal stress; r_w is the radius of the hole; r is the distance from the hole center to the measurement point; P_w is the injection pressure in the hole; P_b is the breakdown pressure; E is Young's modulus; v is Poisson's ratio; σ_{ri} is radial induced stress; $\sigma_{\theta i}$ is tangential induced stress; ε_{ri} is the radial induced strain; $\varepsilon_{\theta i}$ is the tangential induced strain; θ is the angle between the line between the measurement point and the center of the hole and the direction of the maximum principal stress.

2.2 Flow Equations

In hydraulic fracturing, intra-fracture fluid pressure serves as the primary energy source for fracture expansion. Assuming the fracturing fluid is incompressible and neglecting the impacts of fluid inertia and fracture wall roughness, flow within the viscous domain is categorized into tangential flow along the viscous unit and normal flow perpendicular to the viscous unit, as illustrated in Figure 2.

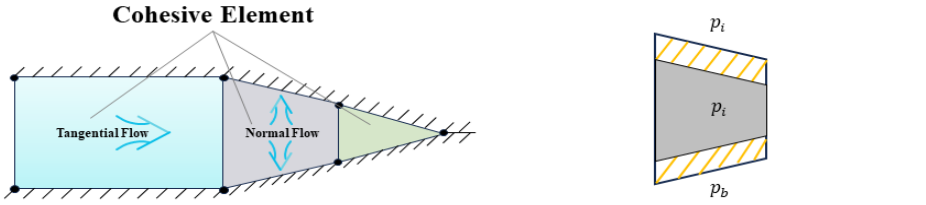

(a) Flow within cohesive elements (b) Leak-off coefficient interpretation as a permeable layer

Figure 2. The Flow Patterns of Pore Fluid in Cohesive Elements (Ma, 2023)

Tangential flow equations:

Specifically, the flow and pressure gradients in the tangential direction are consistent with the cubic seepage equation, which can be expressed as (Ma et al., 2023):

$$q = -\frac{w^3}{12\mu}\Delta p_f \tag{5}$$

Where q denotes the volume flow rate through the fracture cross-section, w denotes the fracture width that varies continuously with time, μ denotes the viscosity of the fracturing fluid, and Δp_f denotes the fluid pressure gradient along the viscous zone.

Normal flow equation:

Fluid in the fracture flows mainly in the tangential direction, and a small amount of fluid filters out through the normal flow of the fracture to the surface layer above and below the viscous unit. The normal flow of fracturing fluid in a viscous unit is as follows:

$$\begin{aligned} q_t &= c_t(p_f - p_t) \\ q_b &= c_b(p_f - p_b) \end{aligned} \tag{6}$$

Where c_t, c_b denote the filtration loss coefficients of the fracturing fluid in the upper and lower walls of the fracture, respectively; p_f denotes the fluid pressure of the fracturing fluid in the fracture; p_t, p_b denote the pore pressures in the upper and lower walls of the fracture, respectively.

2.3 Elastic-plastic Damage Model for Viscous Units

In this paper, a quadratic correlation function of the nominal stress ratio is utilized to determine if a crack will open. Complete damage is assumed when the sum of the squares of the critical stress ratios is equal to one. This criterion can be expressed as (Li et al., 2017):

$$\left\{\frac{\langle t_n \rangle}{t_n^0}\right\}^2 + \left\{\frac{t_s}{t_s^0}\right\}^2 + \left\{\frac{t_t}{t_t^0}\right\}^2 = 1 \tag{7}$$

Where t_n^0 is the normal critical stress (rock tensile strength); t_s^0 and t_t^0 are the critical shear stresses; and the symbol $\langle\rangle$ indicates that the pure compressive deformation or stress state does not initiate damage.

When the stress state of the unit satisfies the above equation, the unit starts to incur damage, and as the separation displacement continues to increase, both the unit stiffness and the load carrying capacity continue to decrease, and eventually fail completely. By introducing the damage variable D to describe

the unit damage evolution process, the actual stress state of the unit is as follows (Camanho et al., 2003).

$$t_n = \begin{cases} (1-D)\bar{t}_n, & \bar{t}_n \geq 0 \\ \bar{t}_n, & \bar{t}_n < 0 \end{cases}$$
$$t_s = (1-D)\bar{t}_s \tag{8}$$
$$t_t = (1-D)\bar{t}_t$$

Where $\bar{t}_n$, $\bar{t}_s$, and $\bar{t}_t$ are the stress components estimated by the traction separation criterion before the damage; t_n, t_s, and t_t are the actual stresses in the normal direction and the two shear directions, respectively; and D is the damage variable.

Figure 3 illustrates the intrinsic curves depicting the relationship between effective traction and effective displacement in the viscous unit, where E is the unit stiffness with respect to the geometric parameters; δ_m^0 is the effective displacement at the time of the initial damage; and δ_m^f is the effective displacement at the time of complete separation.

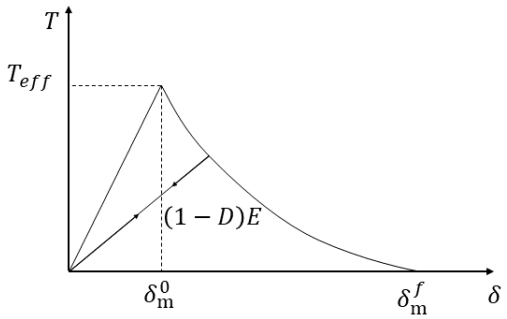

Figure 3. Ontological Relationship Curve of the Cohesion Unit

3. Finite Element Modeling of Dry Hot Rock Fracturing

Experiments, while valuable, are often time-consuming, labor-intensive, and costly. In contrast, numerical simulations offer a more time-efficient, cost-effective, and manageable approach, especially under complex conditions that challenge experimental setups. The finite element method (FEM) has emerged as a particularly effective simulation technique for hydraulic fracturing, as evidenced by its extensive application in the literature (Bao et al., 2014; Chen, 2012; Shauer & Duarte, 2019). Figure 4 illustrates the finite element model, constructed based on the dimensions of the rock samples used in experiments. This model centrally places the injection holes and employs pulse pattern, temperature, geostress differential, and confining pressure as variable parameters to simulate the fracturing process.

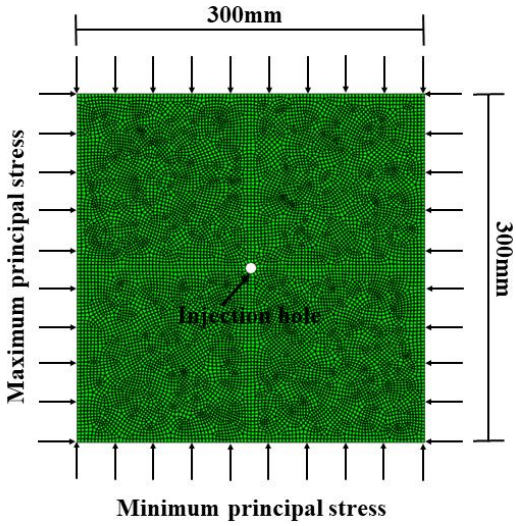

Figure 4. Hydraulic Fracturing Cohesive Element Model

The seepage-stress unit within ABAQUS represents the predominant choice for hydraulic fracturing simulations currently. However, this unit lacks a temperature feature. In response, this study leverages breakdown pressure data of rocks at various temperatures (referenced in Table 1 from existing literature (Cheng et al., 2021)) to calibrate the model's damage intensity. Such calibration facilitates the integration of temperature considerations into the hydraulic fracturing simulation, enabling a more nuanced understanding of the temperature's impact on rock behavior.

Table 1. Fracturing Test Parameters and Breakdown Pressures (Cheng, 2021)

Test No	Injection Flow Rate (ml/min)	Temperature (℃)	Confining stresses (MPa)	Breakdown pressure (MPa)
1	10	30	4/12	30.28
2	10	60	4/12	29.49
3	10	90	4/12	28.32
4	10	120	4/12	25.24
5	10	150	4/12	24.68

3.1 Model Setup and Validation

In the simulations presented in this study, the Abaqus software's pore pressure cohesive unit is employed to model the initiation and extension of hydraulic cracks, as well as the tangential flow of fluid within these cracks and the normal filtration at their surfaces. The model's damage behavior follows the traction-separation criterion, while the fracture criterion is based on the quadratic nominal stress criterion, facilitating the simulation of hydraulic crack propagation. Additionally, the determination of hydraulic crack length and the quantification of damaged units are conducted through post-processing. The essential parameters utilized in the model are detailed in Table 2.

Table 2. Basic Parameters of the Model

Parameter name	parameter value	Parameter name	parameter value
Model size (m)	0.3×0.3	Fracturing fluid viscosity (Pa s)	0.001
Mesh basic dimensions (m)	0.003	Injection length (m)	0.15
Reservoir permeability（mD）	0.034	Cohesive cell thickness (m)	0.001
Reservoir porosity (%)	3.22	Viscosity regularization factor	0.0001
Specific gravity of fracturing fluid (N/m3)	9800	In situ stress (MPa)	4/8/12
Reservoir modulus of elasticity (GPa)	39.99	Initial Pore Ratio	0.033
Reservoir Poisson's ratio	0.28	Fracturing fluid flow (ml/min)	10
Damage intensity (MPa)	8.5/20/20	Reservoir temperature (℃)	150
Unit damage displacement (m)	0.001	Fracturing fluid temperature (℃)	20
Coefficient of leaching	1×10^{-14}	Injection time (s)	1

To ascertain the reliability of our cohesive unit model, we conducted a series of hydraulic fracturing simulations at varying temperatures. The outcomes of these simulations were juxtaposed with laboratory experimental results to confirm the model's validity. Parameters included an injection flow rate of 10 ml/min, a maximum confining pressure of 12 MPa, and a minimum confining pressure of 4 MPa.

Figure 5 illustrates the comparison between the experimental and simulated fracture pressures across varying temperatures, revealing a maximum error of 3.65%. This paper also includes a validation study from Ren et al. on cyclic pulse hydraulic fracturing (Ren et al., 2023), presented in Figure 6, which compares experimental and simulated breakdown pressures under different fracturing modes; here, the discrepancy is reported at 5.47%. Furthermore, similar numerical simulation models have been corroborated by previous studies (Xue et al., 2023; Zhang et al., 2021), which consistently align the simulated values closely with experimental outcomes. These findings affirm that the numerical model is robust and the errors are within acceptable bounds.

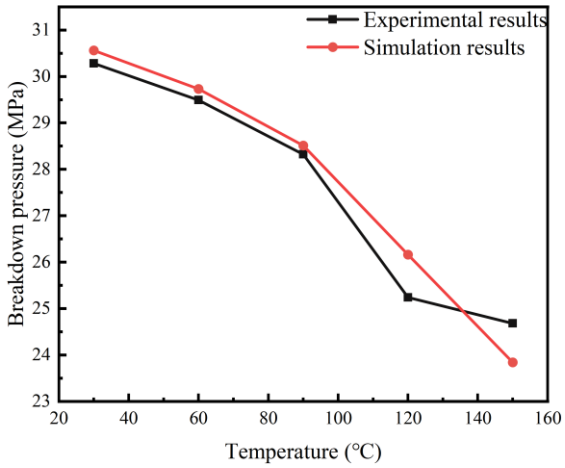

Figure 5. Comparison of Experimental Breakdown Pressure and Simulated Breakdown Pressure at Different Temperatures

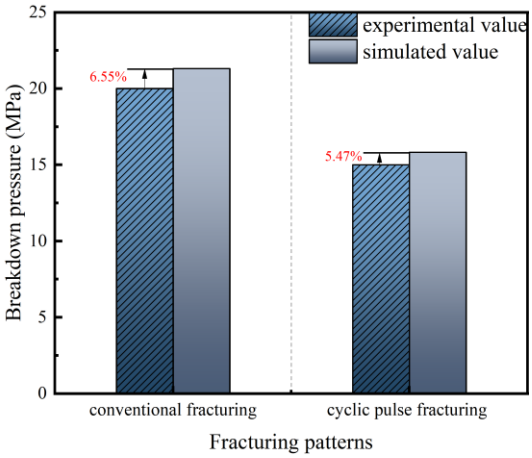

Figure 6. Comparison of Experimental Breakdown Pressure and Simulated Breakdown Pressure under Different Fracturing Modes

3.2 Numerical Simulation of Pulsed Hydraulic Fracturing

Pulse hydraulic fracturing is an emerging technique that offers the advantages of lower fracture initiation pressures and enhanced fracture expansion post-compression, as detailed in references (Gao et al., 2022; Wei et al., 2023). This study investigates four distinct fracturing schemes, depicted in Figure 7. The initial scheme is the conventional injection method, where the injection rate uniformly increases to 10 ml/min within 0-0.2 seconds and then stabilizes. The subsequent schemes—second, third, and fourth—are multi-stage cyclic pulse injection methods. These stages are set to 20%, 40%, 60%, and 80% of the conventional test rate. Initially, the amplitude size of the pulse intervals is set at 10% and 20% of the interval's maximum value, with pulse frequencies of 3 Hz and 5 Hz. The pressure increments during the test proceed as follows: the first stage increases to 20%, the second stage from 20% to 40%, the third stage from 40% to 60%, and the fourth stage from 60% to 80%.

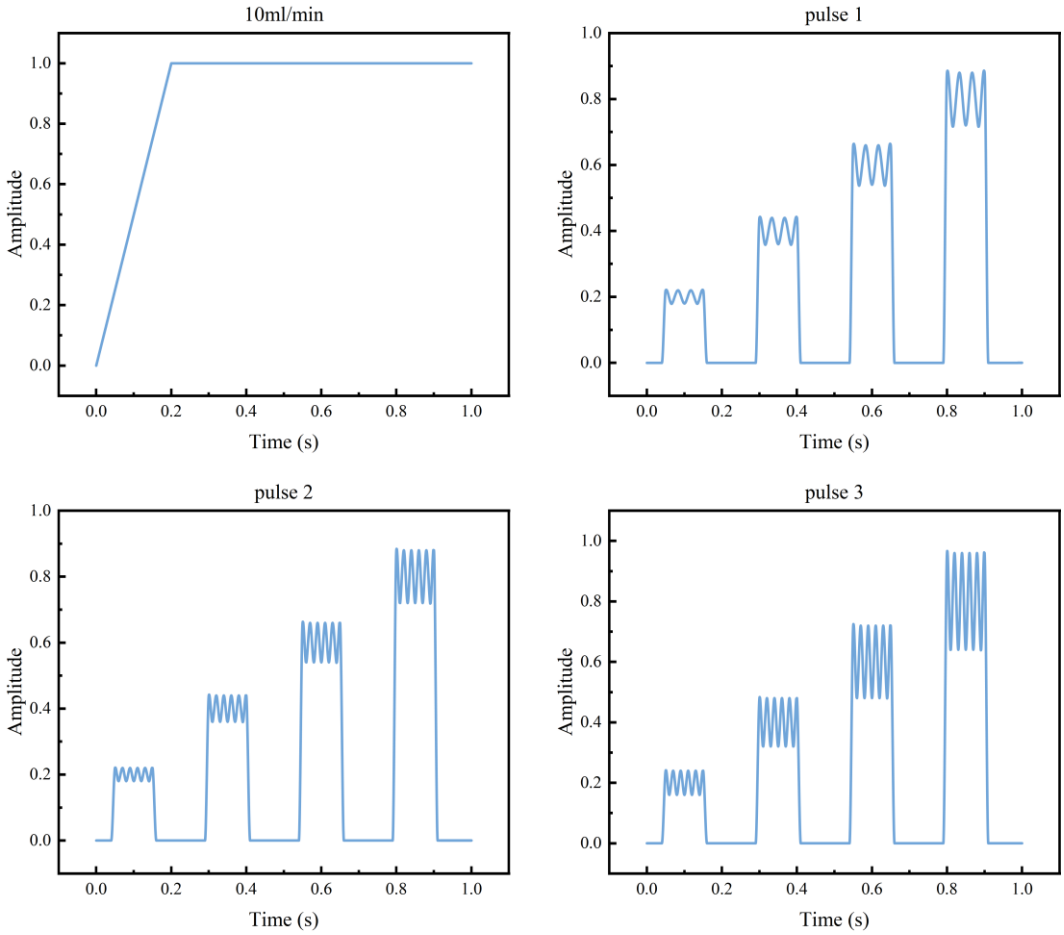

Figure 7. Four Different Injection Schemes Applied in Hydraulic Fracturing Simulations

A total of thirty-two simulation tests, detailed in Table 3, were conducted to examine the hydraulic fracturing characteristics of dry hot rocks, focusing on the influences of pulse pattern, temperature, geostress difference, and confining pressure. Tests 1 to 20 evaluated the effect of pulse pattern on hydraulic fracturing under varying temperature conditions, maintaining a maximum principal stress of 10 MPa and a minimum of 6 MPa, across four fracturing modes: continuous flow at 10 ml/min, Pulse1 (low-frequency, low-amplitude), Pulse2 (high-frequency, low-amplitude), and Pulse3 (high-frequency, high-amplitude). Tests 17 to 28 investigated the impact of geostress difference, maintaining constant temperature and fracturing mode, with three stress ratios examined: 10 MPa/6 MPa, 10 MPa/8 MPa, and 10 MPa/10 MPa. Lastly, tests 25 to 32 assessed the role of confining pressure under uniform temperature and fracturing conditions, exploring two pressure settings: 10 MPa and 6 MPa.

Table 3. Hydraulic Fracturing Simulation Results

Test No	water injection mode	Temperature (℃)	Maximum/minimum principal stress（MPa）	Breakdown pressure (MPa)
1	10ml/min	30	10/6	33.16
2	Pulse 1			30.17
3	Pulse 2			28.60
4	Pulse 3			24.19
5	10ml/min	60		32.43
6	Pulse 1			28.62
7	Pulse 2			26.46
8	Pulse 3			22.66
9	10ml/min	90		29.57
10	Pulse 1			24.95
11	Pulse 2			24.08
12	Pulse 3			19.80
13	10ml/min	120		28.03
14	Pulse 1			23.13
15	Pulse 2			22.33
16	Pulse 3			18.30
17	10ml/min	150		27.55
18	Pulse 1			21.94
19	Pulse 2			19.58
20	Pulse 3			17.17
21	10ml/min	150	10/8	30.78
22	Pulse 1			24.36
23	Pulse 2			23.56
24	Pulse 3			19.11
25	10ml/min	150	10/10	33.55
26	Pulse 1			28.69
27	Pulse 2			26.38
28	Pulse 3			25.18
29	10ml/min	150	6/6	25.03
30	Pulse 1			22.11
31	Pulse 2			20.12
32	Pulse 3			17.29

4. Simulation Results and Analysis

4.1 Effect of Pulse Pattern

The four distinct fracturing schemes employed in this study are illustrated in Figure 7. The first scheme is a conventional injection method, while the subsequent schemes—second, third, and fourth—are multi-stage cyclic pulse injection schemes. These methods were selected based on prior experimental evidence indicating that cyclic injection reduces the magnitude of seismic events. Although the improvement in hydraulic performance is less pronounced than with continuous injection, pulse pressurization effectively enhances permeability (Zhuang et al., 2020).

Figure 8a presents simulation results from tests 1 through 20, demonstrating that the cyclic pulse water injection method significantly reduces the breakdown pressure in hydraulic fracturing of dry hot rock. A comparative analysis between pulse1 and pulse2 shows that increasing the pulse frequency from 3 Hz to 5 Hz further reduces the breakdown pressure. Similarly, an increase in pulse amplitude from 10% to 20% (pulse2 to pulse3) results in additional reductions. At a rock temperature of 150 ℃, modifying the pulse pattern decreases the breakdown pressure from 27.55 MPa to 17.17 MPa, a 37.68% reduction. Furthermore, Figures 8b, c, and d indicate that high-frequency and high-amplitude pulse injections enhance the expansion of the hydraulic fracture network. Specifically, at 150 ℃, the number of fracture rupture units increased from 76 to 121, and the fracture length grew from 234.73 mm to 367.84 mm—both metrics showing more than a 50% increase due to changes in pulse pattern.

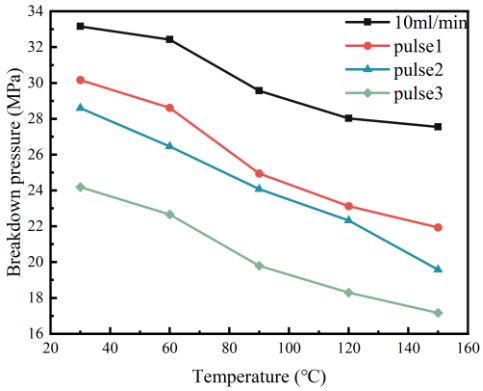

a. Effect of pulse pattern on fracture breakdown pressure

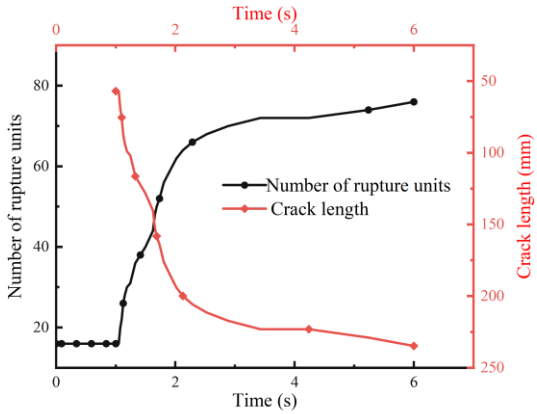

b. Number of fracture rupture units and fracture lengths in pulse1 mode at 150℃

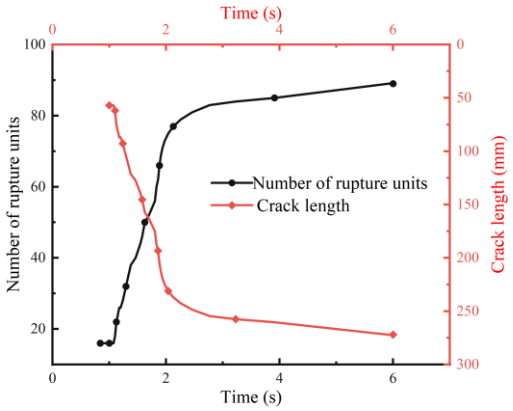

c. Number of fracture rupture units and fracture length in pulse2 mode at 150℃

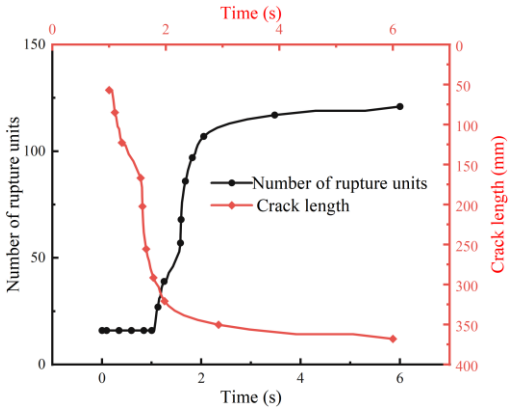

d. Number of fracture rupture units and fracture length in pulse3 mode at 150℃

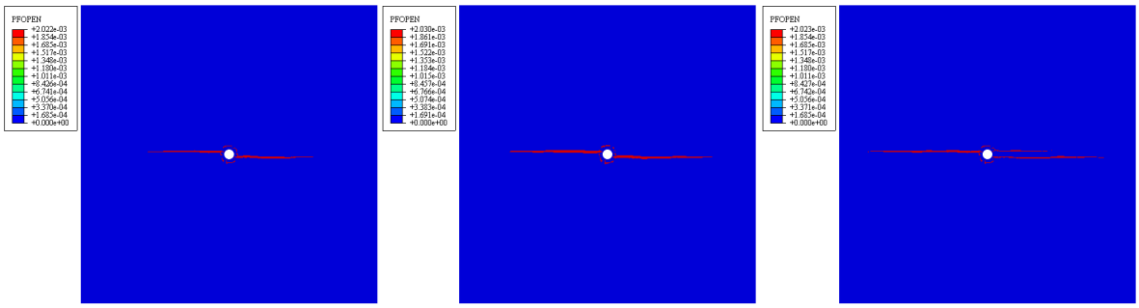

Pulse1 Pulse2 Pulse3

e. Hydraulic fracture under geostress of 6/10MPa at 150℃

Figure 8. Effect of Pulse Pattern on Crack Extension

4.2 Effect of Temperature

Fracturing construction in dry-heat rock formations diverges significantly from conventional hydraulic fracturing due to the unique conditions of high temperature and high pressure in dry-heat environments. Specifically, injecting low-temperature fracturing fluid into a high-temperature formation induces significant thermal stress, which influences the expansion of fractures. Additionally, the impact of this low-temperature fluid varies depending on the rock's mechanical properties, leading to distinct fracture expansion behaviors under thermal stress (Zhang et al., 2023; Zhang et al., 2019).

This study investigates the impact of temperature on the expansion of the fracture network in pulsed hydraulic fracturing within dry hot rock, analyzing fracture pressure, the number of fracture units, and fracture lengths. The model's rock temperatures vary from 30 ℃ to 150 ℃, while the fracturing fluid, maintained at room temperature, creates an increasing temperature differential with the rock as the rock temperature rises. Figure 9a demonstrates that with rising rock temperatures, observed in Tests 1 to 20, the fracture pressure in dry hot rock declines. Furthermore, Figure 9b reveals that as the temperature increases in the pulse1 fracturing mode, the number of fracture units rises from 52 to 76, and fracture lengths extend from 163.97 mm to 234.73 mm. Across the entire fracture network in dry hot rock, higher rock temperatures correlate with longer total fracture lengths when the fracturing fluid

temperature remains constant. The findings indicate that a larger temperature difference between the fracturing fluid and the rock enhances fracture network expansion. Additionally, rock temperature significantly affects the breakdown pressure of granite specimens, with the breakdown pressure decreasing as rock temperature increases under specific injection flow rates, stress conditions, and fracturing modes.

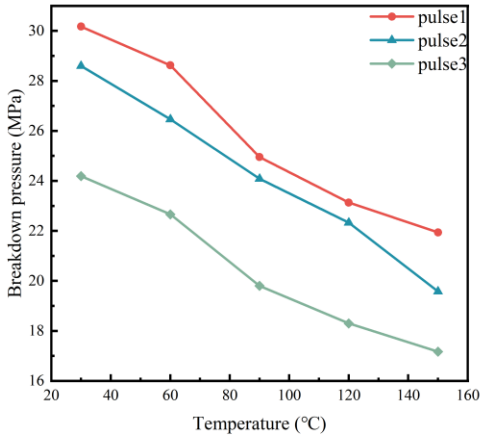

a. Effect of dry hot rock temperature on fracture pressure

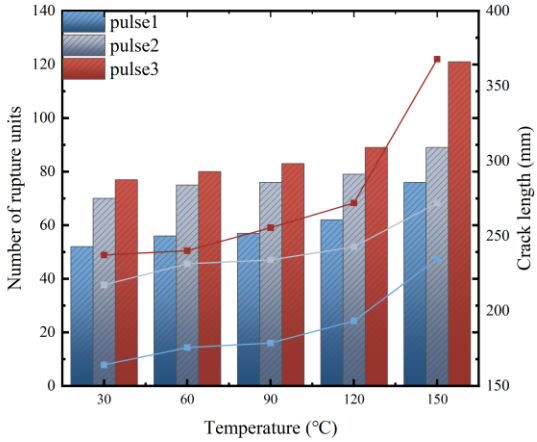

b. Effect of dry hot rock temperature on the number of fracture units and fracture lengths

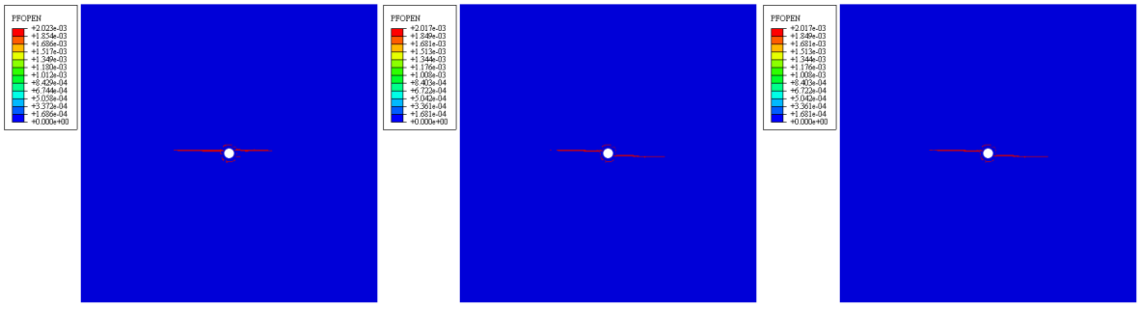

30℃ 60℃ 90℃

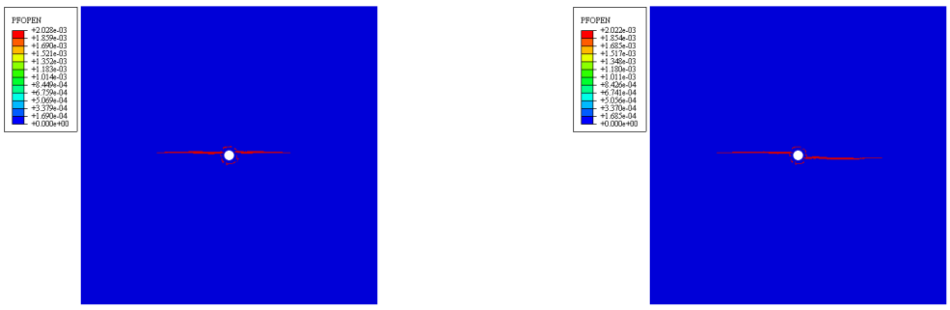

120℃ 150℃

c. Hydraulic cracking in pulse1 pulse mode at different temperatures

Figure 9. Effect of Dry Hot Rock Temperature on Crack Extension

4.3 Effect of Geostress Differential

The impact of geostress differential on pulsed hydraulic fracturing-induced fractures is both complex and significant. Geostress differential arise from variations in formation stresses across different directions. These differentials influence the initiation, propagation, and orientation of fractures during hydraulic fracturing. Notably, fractures tend to propagate towards the direction of the highest principal stress, potentially causing deviations in fracture orientation when significant geostress differences exist. Additionally, geostress differential elevate the fracture pressure required, thereby increasing the volume and cost of the necessary fracturing fluid, and complicating the operation. Moreover, large geostress differential can hasten fracture closure post-operation, diminishing fracture conductivity, and destabilize fractures, making them more prone to premature closure or transformation into other forms. Consequently, understanding the role of geostress differential in hydraulic fracturing demands a thorough assessment of geological conditions, fracturing parameters, and formation stresses.

Figure 10a illustrates the simulation results from Experiments 17 to 28, plotting geostress differential against breakdown pressure on the x-axis and y-axis, respectively. The scatter plots, categorized under four fracturing modes, are presented and analyzed in Figure 10a. It is evident that geostress differential significantly influences fracture extension, with breakdown pressure inversely related to the increase in stress difference (Li et al., 2015). At 150 ℃ in pulse3 mode, the breakdown pressure for dry hot rock is 25.18 MPa at a geostress differential of 0 MPa and decreases to 17.17 MPa at a 4 MPa difference, a reduction of 31.81%.

Figure 10b depicts the expansion of pulse fracturing cracks under varying geostress differential, showing that larger stress differences correlate with more uniform crack morphology, clearer directional tendencies, and a broader main crack extension. At a 4 MPa geostress differential, the maximum geostress direction predominantly influences the fracture extension; at 2 MPa, the fracture morphology around the injection point becomes more complex; and at 0 MPa, fracture morphology exhibits significant randomness. This study confirms that the primary fracture in hydraulic fracturing consistently extends in the direction of the maximum principal stress, favoring the formation of a single flat fracture under high stress differences and a network of fractures under lower stress differences.

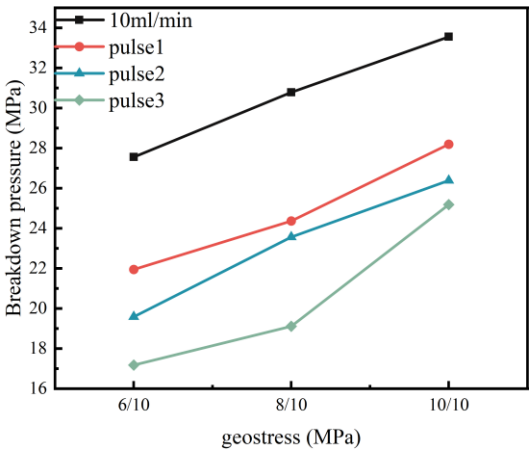

a. The effect of geostress differential on crack breakdown pressure

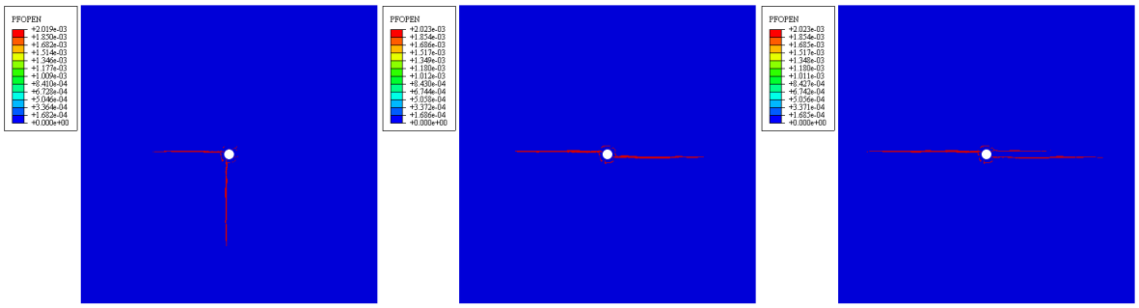

6/10MPa 8/10MPa 10/10MPa

b. Hydraulic cracking in pulse3 pulse mode with different geostress differential at 150 ℃

Figure 10. Effect of Geostress Differential on Crack Extension

4.4 Effect of Confining Pressure

Figure 11a illustrates the simulation results from Experiments 25 to 32, plotting confining pressure against fracture pressure on the y-axis in a bar chart for four fracturing modes. The chart clearly demonstrates that confining pressure significantly impacts crack propagation, evidenced by the increase in fracture pressure as confining pressure rises. Figure 11b depicts at 150 ℃ under the pulse3 mode, a confining pressure of 6 MPa results in two prominent primary cracks along the horizontal direction and an emerging secondary crack vertically; at 10 MPa, a crack develops in both the horizontal and vertical directions.

The analysis reveals that confining pressure's influence on fracture pressure and crack propagation in pulse hydraulic fracturing is a sophisticated physical process. An increase in confining pressure intensifies the stress environment surrounding the rock, consequently elevating the requisite pressure for fracturing. In this dynamic, the confining pressure in the direction of minimum principal stress critically facilitates the initiation and expansion of cracks. Moreover, a rise in confining pressure boosts the rock's elastic modulus, influencing crack propagation. The rock's compressive strength also escalates with confining pressure, necessitating higher pressures for fracturing. Additionally, confining pressure modifies the crack propagation mode, affecting crack length, width, and orientation relative to

the principal stress direction. Typically, higher confining pressures produce straighter and longer cracks, whereas lower pressures lead to more intricate crack pathways. Therefore, confining pressure profoundly affects fracture pressure and crack development during the hydraulic fracturing process.

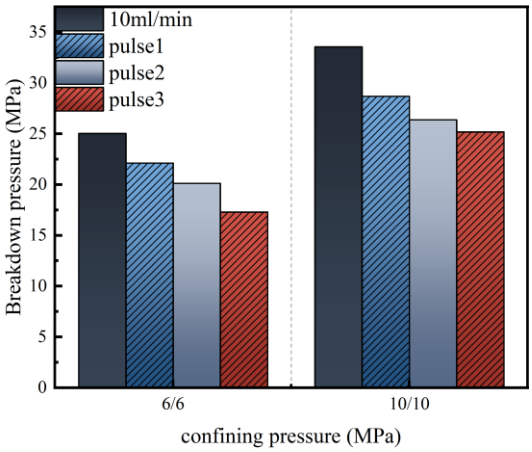

a. Effect of confining pressure on fracture breakdown pressure

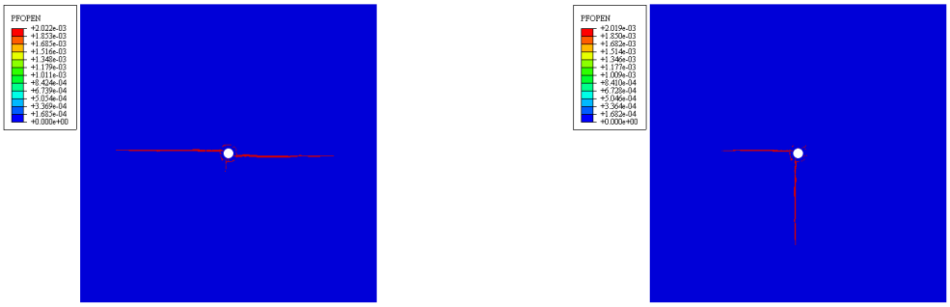

6/6MPa 10/10MPa

b. Hydraulic fracture under different confining pressure pulse3 injection mode at 150℃

Figure 11. Effect of Confining Pressure on Crack Extension

5. Conclusion

Rock fracturing and crack propagation are crucial processes in hydraulic fracturing. In this paper, we investigate the pulsed hydraulic fracturing of hot dry rock by varying the pulsing pattern, temperature, geostress differential, and confining pressure. Based on the analysis of simulation results, the following conclusions can be drawn:

(1) The employment of cohesive elements in hydraulic fracturing simulations offers a detailed and reliable methodology for analyzing and predicting rock fracturing behaviors. This cohesive element model utilizes a second-order stress criterion to assess the initiation of fractures. It incorporates a damage variable, D, to delineate the damage evolution within units, taking into account the rock's microstructure and crack development. Consequently, the model accurately depicts the initiation, expansion, and failure processes of cracks at a microscopic scale, enhancing the realism of rock fracture simulations.

(2) Compared to traditional hydraulic fracturing, pulsed hydraulic fracturing offers several distinct advantages. This technique can significantly reduce the breakdown pressure in hot dry rocks, achieving reductions up to 37.68% under specific conditions. Notably, at constant amplitude, increased frequency exacerbates damage to hot dry rocks; conversely, at constant frequency, higher amplitudes result in greater damage. Pulsed hydraulic fracturing not only improves the efficiency of fracturing but also fosters the development of a more intricate network of fractures. Furthermore, this method has the potential to lessen environmental impacts.

(3) In the pulse hydraulic fracturing of hot dry rocks, the temperature differential between the fracturing fluid and the rocks markedly influences the breakdown pressure. As the rock temperature in the model escalates from 30 ℃ to 150 ℃, the breakdown pressure decreases by approximately 30%. Notably, the introduction of cold water into a high-temperature geothermal reservoir triggers a thermal shock effect. This effect significantly accelerates the initiation and expansion of fractures within the reservoir, thereby enhancing the effectiveness of fracturing in the hot dry rock reservoir.

(4) The impact of geostress differential and confining pressure on pulsed hydraulic fracturing in hot dry rocks is multifaceted, influencing not only the breakdown pressure and the morphology of the fracture face, but also the direction of fracture propagation and the aperture size. Studies have shown that an increase in geostress differential leads to a gradual decrease in breakdown pressure. In high-frequency, high-amplitude pulsed fracturing scenarios, fracture length can extend by up to 50%. Conversely, an increase in confining pressure results in higher breakdown pressure and more complex fracture propagation paths.

Acknowledgments

This work was supported by the National Natural Science Foundation of China (NSFC) [grant numbers 42172274, 42141013, 42002258]; the Scientific Research Project of Education Department of Jilin Province (JJKH20241289KJ).

References

Bao, J. Q., Fathi, E., & Ameri, S. (2014). A coupled finite element method for the numerical simulation of hydraulic fracturing with a condensation technique. *Engineering Fracture Mechanics*, *131*, 269-281. https://doi.org/10.1016/j.engfracmech.2014.08.002

Camanho, P. P., Davila, C. G., & de Moura, M. F. (2003). Numerical Simulation of Mixed-Mode Progressive Delamination in Composite Materials. *Journal of Composite Materials*, *37*(16), 1415-1438. https://doi.org/10.1177/0021998303034505

Chang, X., Xu, E., Guo, Y., Yang, C., Hu, Z., & Guo, W. (2022). Experimental study of hydraulic fracture initiation and propagation in deep shale with different injection methods. *Journal of Petroleum Science and Engineering*, *216*. https://doi.org/10.1016/j.petrol.2022.110834

Chen, Z. (2012). Finite element modelling of viscosity-dominated hydraulic fractures. *Journal of Petroleum Science and Engineering*, *88-89*, 136-144. https://doi.org/10.1016/j.petrol.2011.12.021

Cheng, Y., Zhang, Y., Yu, Z., & Hu, Z. (2021). Investigation on Reservoir Stimulation Characteristics in Hot Dry Rock Geothermal Formations of China During Hydraulic Fracturing. *Rock Mechanics and Rock Engineering*, *54*(8), 3817-3845. https://doi.org/10.1007/s00603-021-02506-y

Frash, L. P., Gutierrez, M., & Hampton, J. (2015). Laboratory-Scale-Model Testing of Well Stimulation by Use of Mechanical-Impulse Hydraulic Fracturing. *SPE Journal*, *20*(03), 536-549. https://doi.org/10.2118/173186-pa

Gao, X., Shi, Y., Shen, C., & Wang, W. (2022). Experimental investigation on hydraulic fracturing under self-excited pulse loading. *Environmental Earth Sciences*, *81*(11). https://doi.org/10.1007/s12665-022-10438-1

Gong, L., Han, D., Chen, Z., Wang, D., Jiao, K., Zhang, X., & Yu, B. (2023). Research status and development trend of key technologies for enhanced geothermal systems. *Natural Gas Industry B*, *10*(2), 140-164. https://doi.org/10.1016/j.ngib.2023.01.011

Jiang-zhan, C., Han, C., Ping-he, S., & Jing-jing, W. (2017). Mechanisms of fracture extending in coal rock by pulse hydraulic fracturing under triaxial loading. *Rock and Soil Mechanics*, *38*(4), 1023-1031.

Kang, H., Zhang, J., Fan, X., Huang, Z., & Li, X. (2020). Cyclic Injection to Enhance Hydraulic Fracturing Efficiency: Insights from Laboratory Experiments. *Geofluids*, *2020*, 1-10. https://doi.org/10.1155/2020/8844293

Li, J., Qiu, Z., Song, D., Zhong, H., & Tang, Z. (2017). Numerical simulation of 3D fracture propagation in wellbore strengthening conditions. *Journal of Petroleum Science and Engineering*, *156*, 258-268. https://doi.org/10.1016/j.petrol.2017.06.010

Li, S., Ma, R., Xu, M., & Xu, G. (2015). Influence of ground stress deviation on coal seam hydraulic fracturing. *Saf. Coal Mines*, *46*, 140-144.

Ma, J., Li, X., Yao, Q., & Tan, K. (2023). Numerical simulation of hydraulic fracture extension patterns at the interface of coal-measure composite rock mass with Cohesive Zone Model. *Journal of Cleaner Production*, *426*. https://doi.org/10.1016/j.jclepro.2023.139001

Ren, Z., Wang, S., Dong, K., Yu, W., & Lu, L. (2023). Exploring the Mechanism of Pulse Hydraulic Fracturing in Tight Reservoirs. *Processes*, *11*(12). https://doi.org/10.3390/pr11123398

Safari, R., Gandikota, R., Mutlu, O., Ji, M., Glanville, J., & Abass, H. (2015). Pulse Fracturing in Shale Reservoirs: Geomechanical Aspects, Ductile/Brittle Transition, and Field Implications. *SPE Journal*, *20*(06), 1287-1304. https://doi.org/10.2118/168759-pa

Shauer, N., & Duarte, C. A. (2019). Improved algorithms for generalized finite element simulations of three-dimensional hydraulic fracture propagation. *International Journal for Numerical and Analytical Methods in Geomechanics*, *43*(18), 2707-2742. https://doi.org/10.1002/nag.2977

Wei, C., Li, S., Yu, L., Zhang, B., Liu, R., Pan, D., & Zhang, F. (2023). Study on Mechanism of Strength Deterioration of Rock-Like Specimen and Fracture Damage Deterioration Model Under Pulse Hydraulic Fracturing. *Rock Mechanics and Rock Engineering*, *56*(7), 4959-4973. https://doi.org/10.1007/s00603-023-03313-3

Wu, X. X., Shi, S. M., Zhao, P., Wei, H. B., Zhang, L., & Bai, X. M. (2012). The Prediction for Favorable Areas of Hot Dry Rock Exploration in the Northern Part of Songliao Basin. *Advanced Materials Research*, *616-618*, 109-115. https://doi.org/10.4028/www.scientific.net/AMR.616-618.109

Xue, Y., Liu, S., Chai, J., Liu, J., Ranjith, P. G., Cai, C., Gao, F., & Bai, X. (2023). Effect of water-cooling shock on fracture initiation and morphology of high-temperature granite: Application of hydraulic fracturing to enhanced geothermal systems. *Applied Energy*, *337*. https://doi.org/10.1016/j.apenergy.2023.120858

Yang, Y., Chen, F., Yu, S., Zheng, Y., He, S., Zeng, Y., Xie, X., Zhu, J., & Luo, N. (2023). Investigating the Formation of Hot-Dry Rock in Gonghe Basin, Qinghai, China. *Minerals*, *13*(8). https://doi.org/10.3390/min13081103

Zang, A., Yoon, J. S., Stephansson, O., & Heidbach, O. (2013). Fatigue hydraulic fracturing by cyclic reservoir treatment enhances permeability and reduces induced seismicity. *Geophysical journal international*, *195*(2), 1282-1287. https://doi.org/10.1093/gji/ggt301

Zhang, B., Guo, T., Qu, Z., Wang, J., Chen, M., & Liu, X. (2023). Numerical simulation of fracture propagation and production performance in a fractured geothermal reservoir using a 2D FEM-based THMD coupling model. *Energy*, *273*. https://doi.org/10.1016/j.energy.2023.127175

Zhang, X., Zhang, Y., & Lian, H. (2021). Experimental and Numerical Investigation on Basic Law of Dense Linear Multihole Directional Hydraulic Fracturing. *Geofluids*, *2021*, 1-19. https://doi.org/10.1155/2021/8355737

Zhang, Y., Ma, Y., Hu, Z., Lei, H., Bai, L., Lei, Z., & Zhang, Q. (2019). An experimental investigation into the characteristics of hydraulic fracturing and fracture permeability after hydraulic fracturing in granite. *Renewable Energy*, *140*, 615-624. https://doi.org/10.1016/j.renene.2019.03.096

Zhuang, L., Jung, S. G., Diaz, M., Kim, K. Y., Hofmann, H., Min, K.-B., Zang, A., Stephansson, O., Zimmermann, G., & Yoon, J.-S. (2020). Laboratory True Triaxial Hydraulic Fracturing of Granite Under Six Fluid Injection Schemes and Grain-Scale Fracture Observations. *Rock Mechanics and Rock Engineering*, *53*(10), 4329-4344. https://doi.org/10.1007/s00603-020-02170-8

Zimmermann, G., Zang, A., Stephansson, O., Klee, G., & Semiková, H. (2018). Permeability Enhancement and Fracture Development of Hydraulic In Situ Experiments in the Äspö Hard Rock Laboratory, Sweden. *Rock Mechanics and Rock Engineering*, *52*(2), 495-515. https://doi.org/10.1007/s00603-018-1499-9